Letter

Engineering the geometric optics limit of wave-packet reflection from a planar interface

Sajjad Bashiri,[1,*] Yahong Chen ,[2,3] and Sergey A. Ponomarenko [1,4]

[1]*Department of Electrical and Computer Engineering, Dalhousie University, Halifax, Nova Scotia, Canada B3J 2X4*
[2]*School of Physical Science and Technology, Soochow University, Suzhou 215006, China*
[3]*Suzhou Key Laboratory of Intelligent Photoelectric Perception, Soochow University, Suzhou 215006, China*
[4]*Department of Physics and Atmospheric Science, Dalhousie University, Halifax, Nova Scotia, Canada B3H 4R2*

(Received 5 April 2026; accepted 12 June 2026; published 6 July 2026)

Goos-Hänchen (GH) and Imbert-Fedorov (IF) shifts of paraxial wave packets in reflection from a planar interface, known collectively as optical shifts, appear inevitable within the framework of the wave theory. Yet, we demonstrate that such shifts can be completely eliminated at a given angle of incidence at a planar interface of homogeneous dielectric and absorbing media by classically entangling phase-space degrees of freedom of an incident wave packet. Thus, we can attain a geometric optics limit in the wave-packet reflection from a single planar interface. We identify a set of plasmonic materials (noble metals) and a parameter regime for which such cancellation is robust to modest errors in the incidence angle and source coherence, as well as polarization, providing practical guidelines for tailoring transverse beam displacements and angular deviations with standard metallic coatings.

DOI: 10.1103/gwhv-fj1q

Introduction— A paraxial light wave packet reflected from a planar interface separating two homogeneous media manifests small but measurable shifts of its intensity centroid relative to the geometric optics prediction. The in-plane and out-of-plane displacements are known as the Goos-Hänchen (GH) and Imbert-Fedorov (IF) shifts and arise from the angle-dependent Fresnel phase and polarization mixing at the interface [1–4]. Such optical shifts have been linked to spin-orbit coupling of light and the optical spin Hall effect [5–8]. Analogous GH/IF-type shifts have now been predicted and observed for neutrons, x-rays, electrons, graphene quasiparticles, spin waves, atom optics, matter waves, and temporal boundaries [9–17], and they are increasingly viewed as members of a broader spin-Hall family [18]. In addition, weak-measurement techniques enable subwavelength readout of GH/IF shifts and the spin-Hall effect of light [19–21], which have been exploited in sensing, imaging, and edge-enhancement schemes based on enhanced GH or spin-Hall responses [22–26].

Recent work has unveiled a fundamental link between a previously unrecognized type of classical entanglement—theoretically discovered in Ref. [27] and recently studied experimentally in Ref. [28]—namely, the phase-space nonseparability of a light source, and spatial optical shifts of the wave packets generated by the source and reflected from a planar interface [29]. A twisted Gaussian Schell-model (TGSM) beam provides a convenient and analytically tractable framework to describe light sources with tunable phase-space nonseparability [27,30–34]. Using TGSM beams as a representative example, the authors of Ref. [29] demonstrated that the phase-space nonseparability introduces additional contributions to both GH and IF shifts under partial reflection at a lossless interface. In particular, the IF shift of circularly polarized beams can be canceled at a specific angle of incidence by tuning the source phase-space nonseparability, for instance through the twist parameter or coherence length. At the same time, the GH shift typically arises under the condition of total internal reflection and therefore cannot be eliminated at a lossless interface. However, if at least one of the homogeneous media is absorbing, such as a metal reflector with a complex refractive index, the situation becomes less clear. Absorption and longitudinal field components can, in general, produce large GH shifts and a pronounced polarization dependence of the IF shifts [35–37]. Patterned metal films and metasurfaces can further yield giant spatial and angular shifts near the surface-plasmon or bound-state-in-continuum resonances [23,38–40]. This raises two questions. First, to what extent can we systematically control the spatial GH and IF shifts at a single dielectric-absorber interface, such as a simple metal coating? At a more fundamental level, can one simultaneously cancel all spatial and angular shifts at the same incidence angle, thereby realizing a geometric optics limit in wave-packet reflection from a simple interface?

In this Letter, we apply the analytical phase-space theory advanced in Ref. [29] to study optical shifts of phase-space nonseparable wave packets reflected from a simple air-metal interface (metal coating). We stress that although we use the TGSM beam as a representative example, our findings are equally applicable to other wave packets with classically entangled phase-space degrees of freedom, such as fully coherent beams endowed with orbital angular momentum. We demonstrate that the phase-space nonseparability of the source beam enables *spatial* GH and IF shift control at the

*Contact author: s.bashiri@dal.ca

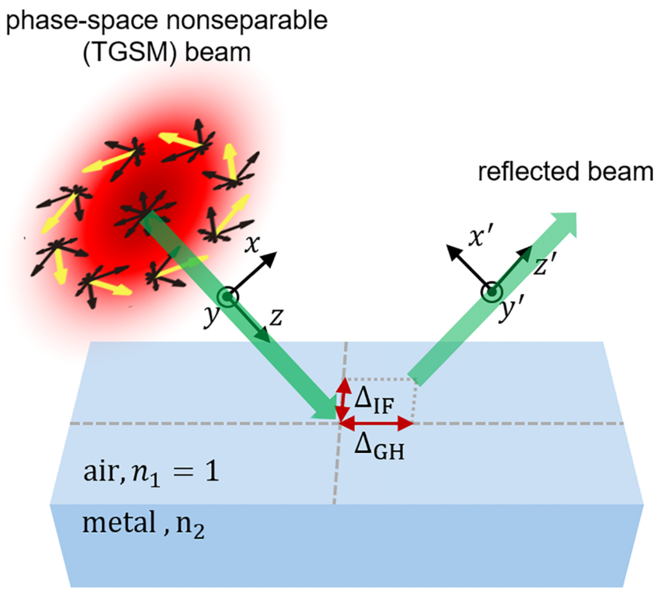

FIG. 1. Schematic of a phase-space nonseparable TGSM beam reflected from an air-metal interface. In the source cross section, the black arrows denote the local distribution of transverse wave vectors at different transverse positions, while the yellow arrows mark the corresponding central local transverse wave-vector directions; their azimuthal handedness is set by the sign of the twist parameter t. The green arrows show the incident and reflected beam axes, and the red arrows indicate the spatial GH and IF shifts.

interface. We show that for a broad class of metal coatings, the GH shift can be canceled at a certain angle of incidence. We also show that spatial GH and IF shifts can be suppressed at the *same* incidence angle for many coatings, including aluminum and copper ones. At the same time, we find that the angular shifts can also be jointly suppressed at the same incidence angle for which the spatial shifts are canceled by adjusting the coherence and polarization state of the TGSM source. Thus, we can engineer a geometric optic limit in reflection. We identify simple polarization-coherence design rules that allow for simultaneous suppression and sign reversal of the spatial optical shifts which are tolerant to modest errors in the incidence angle and source's coherence and polarization. This work provides a demonstration of coherence-controlled joint suppression of spatial and angular GH and IF shifts at a simple air-metal interface.

Theoretical framework— We consider a paraxial phase-space nonseparable wave packet of vacuum wavelength λ_0 incident from air ($n_1 = 1$) on a homogeneous isotropic substrate with a complex refractive index n_2 as sketched in Fig. 1. Hereafter, it will prove convenient to introduce a set of basis unit vectors, $\{\mathbf{e}'_x, \mathbf{e}'_y, \mathbf{e}'_z\}$, associated with a reflected beam (primed). The source is a polarized, twisted Gaussian Schell-model (TGSM) beam with rms width σ_I and transverse coherence length σ_c. These define the dimensionless coherence parameters $\xi_c = \sigma_c/\sigma_I$ and twist $t = u\sigma_c^2$ [27], which together control the phase-space nonseparability of the source. We further introduce $k = 2\pi n_1/\lambda_0$ and the Rayleigh range associated with σ_I as $z_R = k\sigma_I^2$. The source polarization is characterized by the Jones vector $\mathbf{a} = (a_x, a_y)$ in a coordinate frame associated with the incident beam (unprimed); we assume $a_x = |a_x|$ and $a_y = |a_y|\mathrm{e}^{i\delta}$ unless stated otherwise.

Let θ be an incidence angle and $r_{p,s}(\theta) = |r_{p,s}(\theta)|e^{i\phi_{p,s}(\theta)}$ the complex Fresnel reflection coefficients for p and s polarizations (see Supplemental Material [41]). Following the phase-space treatment of Ref. [29], we can write for the centroid of the reflected TGSM beam the expression

$$\mathbf{R}(z') = \boldsymbol{\Delta} - \frac{2t}{\xi_c^2}\boldsymbol{\Lambda} + \frac{2z'}{z_R\xi_c^2}\left(1 + \frac{\xi_c^2}{4} + \frac{t^2}{\xi_c^2}\right)\boldsymbol{\Theta}, \qquad (1)$$

where $\boldsymbol{\Delta}$, $\boldsymbol{\Lambda}$, and $\boldsymbol{\Theta}$ are two-dimensional vectors containing the x and y components. Their explicit forms, expressed in terms of the angular blocks $X_{p,s}(\theta)$ and $Y_{p,s}(\theta)$, are provided in the Supplemental Material [41]. The first term on the right-hand side represents the intrinsic spatial shifts. It contains both GH and IF contributions for total internal reflection at a lossless interface or for reflection from lossy metal surfaces [44], while under partial reflection at a lossless interface it contains only the IF shift (for circularly polarized beams). The second term describes the contribution arising from the phase-space nonseparability of the source, which depends on the twist parameter t and the coherence parameter ξ_c. This contribution vanishes under total internal reflection at a lossless interface [29] but generally possesses nonzero x and y components under partial reflection or at an air-metal interface (due to the complex refractive index of the substrate) [41]. Here, we find that, because neither the intrinsic nor the nonseparability-induced components vanish at an air-metal interface, phase-space nonseparability provides an additional degree of freedom for engineering (enhancing or canceling) both the spatial GH and IF shifts. The last term in Eq. (1) represents the contribution from the angular shifts, which grows linearly with the propagation distance z' and depends on both the polarization state and the phase-space nonseparability of the incident beam. Thus, the angular shifts can also be controlled.

Spatial GH shift suppression at a metal mirror— We display the spatial GH and IF shifts of a linearly polarized TGSM beam incident at an air-aluminum interface in Fig. 2. The spatial shifts of the beam for positive (negative) t correspond to solid (dashed) curves in Fig. 2. We can see in the figure that while IF shifts cross the zero line for both positive and negative values of the twist parameter, the GH shifts do so only for positive t. In Fig. 2, we also display the spatial shifts (solid black curves) for phase-space separable Gaussian Schell-model wave packets with no twist ($t = 0$). These shifts are determined by the intrinsic terms associated with $\boldsymbol{\Delta}$ and hence the shifts cannot be controlled in this case.

In Fig. 3 we show spatial shifts of TGSM beams reflected from aluminum ($n_2 = 1.37 + 7.62i$), copper ($n_2 = 0.239 + 3.43i$), and gold ($n_2 = 0.18 + 3.43i$) coatings at $\lambda_0 = 633$ nm. In both panels of the figure, we fix the beam parameters to be $t = 0.80$, $\xi_c = 0.50$, and $\sigma_I = 1$ mm, and compare the analytical prediction (solid curves) with coherent-mode simulations (markers) carried out following the numerical procedure described in the Supplemental Material to Ref. [29]. Figure 3(a) corresponds to a linearly polarized incident beam with $|a_x| = |a_y| = 1$ and $\delta = 0^\circ$. For all three metals, $\Delta_{\mathrm{GH}}(\theta)$ starts from zero at normal incidence, attains

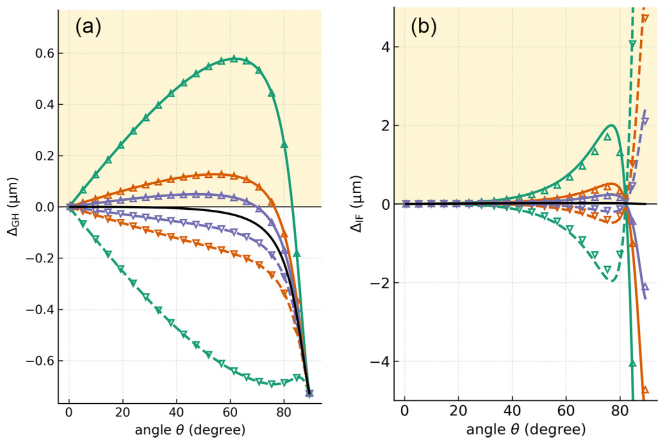

FIG. 2. Spatial GH and IF shifts of linearly polarized TGSM beams reflected from an aluminum mirror at $\lambda_0 = 633$ nm. (a) $\Delta_{GH}(\theta)$; (b) $\Delta_{IF}(\theta)$. Colored solid and dashed curves show the analytical predictions, while triangle markers show numerical TGSM coherent-mode results. Colors encode the coherence parameter: green, $\xi_c = 0.1$; orange, $\xi_c = 0.2$; purple, $\xi_c = 0.3$. For each ξ_c, the upper (lower) branch corresponds to $t = +0.8$ $(t = -0.8)$. The black solid curve shows the analytical result for $t = 0$, corresponding to the intrinsic terms Δ_x in (a) and Δ_y in (b).

a positive maximum at moderate incidence angles, before crossing the line $\Delta_{GH} = 0$ and taking on large negative values within the grazing incidence regime. The vertical dashed lines indicate zero-crossing angles. In Fig. 3(b), we display $\Delta_{GH}(\theta)$ for an elliptically polarized input beam with $|a_x| = 1.0$, $|a_y| = 0.85$, and $\delta = 45^\circ$. The overall functional dependence of Δ_{GH} on θ is preserved, while the zero-crossing angle shifts and the magnitude of $\Delta_{GH}(\theta)$ for larger incidence angles is reduced, so that $\Delta_{GH}(\theta)$ remains closer to zero over a wider angular range. In both panels, numerical simulations closely track the analytical curves for all three metal coatings.

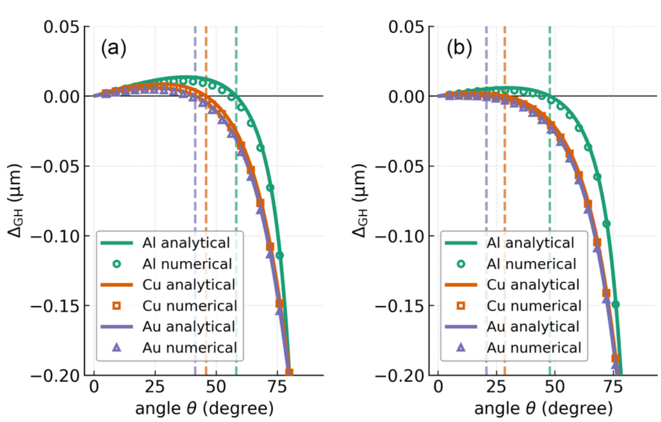

FIG. 3. Spatial GH shift $\Delta_{GH}(\theta)$ for TGSM beams reflected from aluminum, copper, and gold mirrors at $\lambda_0 = 633$ nm. Solid lines: analytical prediction from Eq. (1). Markers: TGSM coherent-mode simulations. Vertical dashed lines mark the single zero crossing of Δ_{GH} for each metal. (a) corresponds to a linear polarization with $|a_x| = |a_y| = 1.0$ and $\delta = 0^\circ$. (b) corresponds to an elliptical polarization with $|a_x| = 1.0$, $|a_y| = 0.85$, and $\delta = 45^\circ$. In both panels, the beam parameters are $t = 0.80$, $\xi_c = 0.50$, and $\sigma_I = 1$ mm.

The three mirrors show systematic differences. Among the three mirrors, aluminum exhibits the largest positive peak and the most pronounced negative tail, indicating the strongest overall GH response. Copper and gold produce smaller excursions: Their positive peaks are more modest and the curves remain closer to zero over a wider angular range, with gold yielding the smallest overall spatial shift. Thus, for fixed TGSM parameters, the choice of metal coating provides an additional degree of control over the magnitude and sign of Δ_{GH}. These trends admit a simple explanation in terms of the properties of the Fresnel coefficients and the amplitude ratio of the polarization components of the source beam. The peak and sign of the spatial GH shift are governed by the phase derivatives $\partial_\theta \phi_{p,s}$ of the Fresnel coefficients and the relative weights $I_p \propto |a_x|^2 |r_p|^2$ and $I_s \propto |a_y|^2 |r_s|^2$, through polarization-weighted Fresnel complexes in the x component of $\mathbf{\Delta}$, i.e., $\Delta_{x'}$. Metals with larger real and a smaller imaginary part of the refractive index exhibit a stronger incidence angle dependence of the phases of their Fresnel coefficients and hence greater $\Delta_{x'}$, while mirrors made with strongly absorbing materials (large imaginary part for n_2) maintain flatter phases that suppress the shift. At the same time, the ratio $|r_p|^2/|r_s|^2$ differs for Al, Cu, and Au, such that the balance between the p and s channels in $\Delta_{x'}$ and $\Lambda_{x'}$ changes from one metal to another, shifting both the peak amplitude and zero-crossing angle. From an experimental perspective, these curves suggest simple design rules. If we require a large positive GH bump at moderate angles (for example, to enhance a weak-value-type signal), aluminum is the most favorable among the three mirrors. If, instead, one wants to minimize centroid wander and keep the spatial GH shift small (e.g., for a reference mirror in a precision alignment stage), a gold coating is preferable. Having established how material choice and polarization tune the spatial GH response, we now show that the same control parameters can be chosen to ensure simultaneous spatial GH/IF cancellation at a single incidence angle.

Simultaneous cancellation of spatial GH and IF shifts—At the interface ($z' = 0$), Eq. (1) reduces to a purely spatial centroid shift. The intrinsic terms $\mathbf{\Delta}$ and the twist-coherence contributions $\mathbf{\Lambda}$ depend on the longitudinal/transverse kernels $X_{p,s}$ and $Y_{p,s}$ and on the complex polarization product $a_x^* a_y$ (see Supplemental Material [41]), so that we can tune both the magnitude and sign of the spatial shifts by jointly manipulating the twist-coherence and polarization state of the source.

In Fig. 4, we show spatial GH/IF control for TGSM beams reflected from copper at $\lambda_0 = 633$ nm. Solid curves are analytical predictions from Eq. (1) at $z' = 0$, and markers are numerical results. The dashed-dotted curves provide a baseline for a standard fully coherent Gaussian beam ($t = 0$, $\xi_c \to \infty$), which does not exhibit joint zeros under identical conditions. By contrast, tuning a_x/a_y, t, and ξ_c enables $\Delta_{GH}(\theta_0) = \Delta_{IF}(\theta_0) = 0$ at a common incidence angle θ_0.

GH and IF angular shifts in the geometric optics limit— It follows from Eq. (1) by expressing the Fresnel reflection coefficients in terms of their moduli and phases that the angular IF shift can be written in the compact form [41]

$$\Theta_{IF}(\theta) = A(t, \xi_c)\frac{[|r_s(\theta)|^2 - |r_p(\theta)|^2]}{N(\theta)} \cot\theta \cos\delta, \quad (2)$$

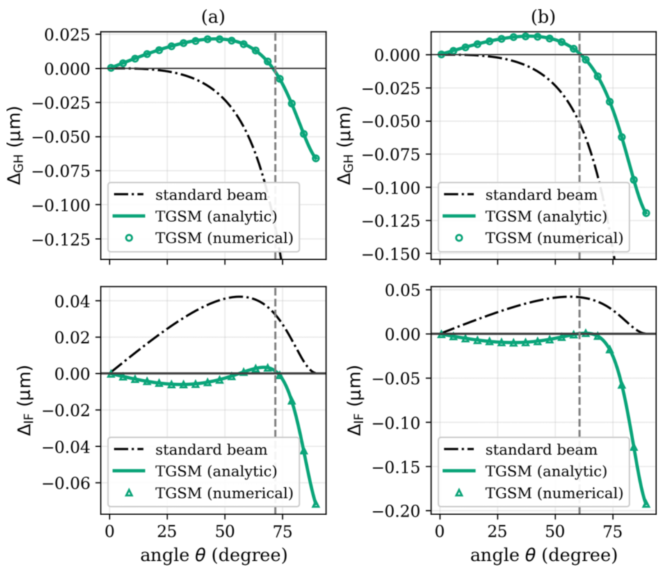

FIG. 4. Spatial Goos-Hänchen and Imbert-Fedorov shifts $\Delta_{\mathrm{GH}}(\theta)$ and $\Delta_{\mathrm{IF}}(\theta)$ for TGSM beams reflected from a copper mirror at $\lambda_0 = 633$ nm. Green solid curves: analytical TGSM predictions [Eq. (1) evaluated at $z' = 0$]. Green markers: TGSM numerical simulation results. Black dashed-dotted curves: baseline shifts for a standard fully coherent Gaussian beam ($t = 0$, $\xi_c \to \infty$) linear polarization. Vertical dashed lines indicate the incidence angles where the TGSM spatial GH and IF shifts vanish simultaneously. (a) $t = 0.80$, $\xi_c = 0.50$, $|a_x| = 0.50$, $|a_y| = 1.10$, $\delta = 90^\circ$. (b) $t = 0.80$, $\xi_c = 0.35$, $|a_x| = 1.00$, $|a_y| = 1.75$, $\delta = 90^\circ$.

where

$$N(\theta) = \frac{|a_x|^2|r_p(\theta)|^2 + |a_y|^2|r_s(\theta)|^2}{|a_x||a_y|}, \tag{3}$$

and a (strictly positive) coherence-twist prefactor is

$$A(t, \xi_c) = \frac{2}{kz_R\xi_c^2}\left(1 + \frac{\xi_c^2}{4} + \frac{t^2}{\xi_c^2}\right). \tag{4}$$

It follows from Eq. (2) that choosing a $\pi/2$ phase offset between the polarization components ($\delta = 90^\circ$) suppresses the angular IF shift for *any* incidence angle, $\Theta_{\mathrm{IF}}(\theta) = 0$. By the same token, the angular GH shift simplifies to

$$\Theta_{\mathrm{GH}}(\theta) = \tfrac{1}{2}A(t, \xi_c)\partial_\theta \ln N(\theta). \tag{5}$$

Thus, after enforcing spatial cancellation at θ_0, the remaining requirement for a full geometrical optic reflection condition is to simultaneously suppress Θ_{GH} at the same θ_0 by a suitable choice of the polarization amplitude ratio. We present an all-shift cancellation scenario in Fig. 5. In our example for an aluminum coating, $|a_x| = 1.3$, $|a_y| = 1.4$, $t = 0.99$, and $\xi_c = 0.40$. We find that $\Delta_{\mathrm{GH}}(\theta_0) = \Delta_{\mathrm{IF}}(\theta_0) = 0$ and $\Theta_{\mathrm{GH}}(\theta_0) = \Theta_{\mathrm{IF}}(\theta_0) = 0$ at $\theta_0 \simeq 23.1^\circ$. We show additional representative examples of all shift cancellation for several metallic coatings in Table 1 of the Supplemental Material [41]. Figure 5 identifies a theoretical cancellation operating point. Although the residual shifts are much smaller than in Fig. 4, nanometer-scale spatial shifts remain within reach of weak-measurement techniques, while the angular signal would generally require additional

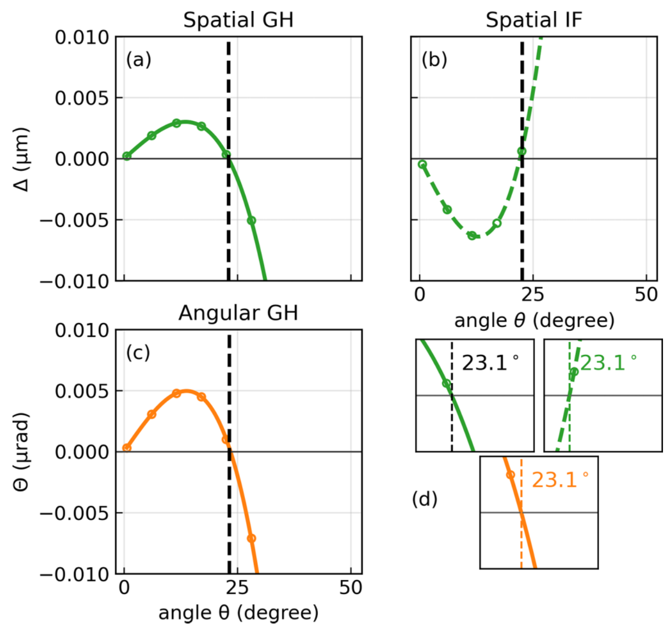

FIG. 5. Four-shift cancellation for a TGSM beam reflected from an aluminum coating at $\lambda_0 = 633$ nm. Top row: (a) spatial Goos-Hänchen and (b) spatial Imbert-Fedorov shifts, $\Delta_{\mathrm{GH}}(\theta)$ and $\Delta_{\mathrm{IF}}(\theta)$ (shown in μm), evaluated at the interface ($z' = 0$). Bottom row: (c) angular Goos–Hänchen shift, $\Theta_{\mathrm{GH}}(\theta)$ (shown in μrad), and (d) close-up of (a)–(c) in the neighborhood of the cancellation point, highlighting the near-simultaneous vanishing of the three nontrivial shifts at $\theta_0 = 23.1^\circ$. For $\delta = 90^\circ$, the angular IF shift vanishes identically, $\Theta_{\mathrm{IF}}(\theta) = 0$, and is therefore not shown as a separate panel. Solid curves show analytical predictions, while markers show numerical results. The beam parameters are $\sigma_I = 1$ mm, $t = 0.99$, $\xi_c = 0.40$, $|a_x| = 1.3$, $|a_y| = 1.4$, and $\delta = 90^\circ$. The vertical dashed lines mark the zero-crossing angles of the corresponding shifts in each subplot; the black dashed line indicates the design point $\theta_0 = 23.1^\circ$ used for the cancellation condition.

amplification or long propagation distance for practical readout.

Conclusions— We have shown that phase-space nonseparability of a twisted Gaussian Schell-model (TGSM) source provides practical control knobs—twist t, coherence ξ_c, and polarization—to tailor, reverse, and simultaneously suppress the Goos-Hänchen (GH) and Imbert-Fedorov (IF) shifts at a simple air-metal interface. For standard metallic coatings (e.g., Al, Cu, Au at $\lambda_0 = 633$ nm), the analytical predictions agree well with coherent-mode simulations and reveal incidence angles where $\Delta_{\mathrm{GH}}(\theta_0) = \Delta_{\mathrm{IF}}(\theta_0) = 0$ at the interface.

Moreover, choosing $\delta = 90^\circ$ suppresses the angular IF deviation for all θ, and, together with an appropriate polarization amplitude ratio and (t, ξ_c) tuning, enables design points where the angular GH deviation is also nulled at the same θ_0, yielding a classical geometric optics limit in wave packet reflection from a simple interface. The resulting polarization-coherence design rules and representative parameter sets provide a practical route to engineering optical-shift cancellation using ordinary metallic reflectors, without resorting to resonant nanostructures. This, in turn, suggests straightforward applications in precision alignment and beam-walk control in folded multimirror optical trains [37,45], calibration and bias suppression in beam-shift metrology (including weak-measurement readout) [19,21,46], compact beam pointing/steering using conventional reflective elements [7,37], and interface refractometry/sensing based on conventional reflective optics [47,48].

Finally, we emphasize that our scheme is experimentally feasible. In particular, recent random-mode superposition approaches have greatly simplified the synthesis of TGSM beams with tunable phase-space nonseparability [28,49]. By engineering the spatial mode distributions and their relative weights, the twist and coherence parameters of TGSM beams can be flexibly controlled, thereby enabling experimental manipulation of both spatial and angular beam shifts. These developments provide a realistic route toward experimental realization of the geometric-optics limit engineered in this work.

Acknowledgment— The authors acknowledge financial support from the National Natural Science Foundation of China (12274310) and the Natural Sciences and Engineering Research Council of Canada (RGPIN-2025-04064).

Data availability— The data that support the findings of this article are not publicly available. The data are available from the authors upon reasonable request.

[1] F. Goos and H. Hänchen, Ein neuer und fundamentaler Versuch zur Totalreflexion, Ann. Phys. **436**, 333 (1947).

[2] F. I. Fedorov, To the theory of total reflection, J. Opt. **15**, 014002 (2013).

[3] C. Imbert, Calculation and experimental proof of the transverse shift induced by total internal reflection of a circularly polarized light beam, Phys. Rev. D **5**, 787 (1972).

[4] J. W. Ra, H. Bertoni, and L. Felsen, Reflection and transmission of beams at a dielectric interface, SIAM J. Appl. Math. **24**, 396 (1973).

[5] M. Onoda, S. Murakami, and N. Nagaosa, Hall effect of light, Phys. Rev. Lett. **93**, 083901 (2004).

[6] K. Y. Bliokh and Y. P. Bliokh, Conservation of angular momentum, transverse shift, and spin Hall effect in reflection and refraction of an electromagnetic wave packet, Phys. Rev. Lett. **96**, 073903 (2006).

[7] K. Y. Bliokh and A. Aiello, Goos–Hänchen and Imbert–Fedorov beam shifts: An overview, J. Opt. **15**, 014001 (2013).

[8] M. Merano, A. Aiello, M. P. van Exter, and J. P. Woerdman, Observing angular deviations in the specular reflection of a light beam, Nat. Photonics **3**, 337 (2009).

[9] V. Ignatovich, Neutron reflection from condensed matter, the Goos–Hänchen effect and coherence, Phys. Lett. A **322**, 36 (2004).

[10] V.-O. de Haan, J. Plomp, T. M. Rekveldt, W. H. Kraan, A. A. van Well, R. M. Dalgliesh, and S. Langridge, Observation of the Goos-Hänchen shift with neutrons, Phys. Rev. Lett. **104**, 010401 (2010).

[11] K. Tamasaku and T. Ishikawa, The Goos–Hänchen effect at Bragg diffraction, Acta Crystallogr. A **58**, 408 (2002).

[12] C. W. J. Beenakker, R. A. Sepkhanov, A. R. Akhmerov, and J. Tworzydło, Quantum Goos-Hänchen effect in graphene, Phys. Rev. Lett. **102**, 146804 (2009).

[13] Z. Wu, F. Zhai, F. M. Peeters, H. Q. Xu, and K. Chang, Valley-dependent Brewster angles and Goos-Hänchen effect in strained graphene, Phys. Rev. Lett. **106**, 176802 (2011).

[14] Y. S. Dadoenkova, N. N. Dadoenkova, I. L. Lyubchanskii, M. L. Sokolovskyy, J. W. Kłos, J. Romero-Vivas, and M. Krawczyk, Huge Goos-Hänchen effect for spin waves: A promising tool for study magnetic properties at interfaces, Appl. Phys. Lett. **101**, 042404 (2012).

[15] J. Huang, Z. Duan, H. Y. Ling, and W. Zhang, Goos-Hänchen-like shifts in atom optics, Phys. Rev. A **77**, 063608 (2008).

[16] S. McKay, V. O. de Haan, J. Leiner, S. R. Parnell, R. M. Dalgliesh, P. Boeni, L. J. Bannenberg, Q. Le Thien, D. V. Baxter, G. Ortiz *et al.*, Observation of a giant Goos-Hänchen shift for matter waves, Phys. Rev. Lett. **134**, 093803 (2025).

[17] S. A. Ponomarenko, J. Zhang, and G. P. Agrawal, Goos-Hänchen shift at a temporal boundary, Phys. Rev. A **106**, L061501 (2022).

[18] M. Kim, Y. Yang, D. Lee, Y. Kim, H. Kim, and J. Rho, Spin Hall effect of light: From fundamentals to recent advancements, Laser Photonics Rev. **17**, 2200046 (2023).

[19] O. Hosten and P. Kwiat, Observation of the spin Hall effect of light via weak measurements, Science **319**, 787 (2008).

[20] P. B. Dixon, D. J. Starling, A. N. Jordan, and J. C. Howell, Ultrasensitive beam deflection measurement via interferometric weak value amplification, Phys. Rev. Lett. **102**, 173601 (2009).

[21] G. Jayaswal, G. Mistura, and M. Merano, Weak measurement of the Goos–Hänchen shift, Opt. Lett. **38**, 1232 (2013).

[22] X. Wang, M. Sang, W. Yuan, Y. Nie, and H. Luo, Optical relative humidity sensing based on oscillating wave-enhanced goos–Hänchen shift, IEEE Photonics Technol. Lett. **28**, 264 (2016).

[23] F. Wu, J. Wu, Z. Guo, H. Jiang, Y. Sun, Y. Li, J. Ren, and H. Chen, Giant enhancement of the Goos-Hänchen shift assisted by quasibound states in the continuum, Phys. Rev. Appl. **12**, 014028 (2019).

[24] T. Zhu, Y. Lou, Y. Zhou, J. Zhang, J. Huang, Y. Li, H. Luo, S. Wen, S. Zhu, Q. Gong *et al.*, Generalized spatial differentiation from the spin Hall effect of light and its application in image processing of edge detection, Phys. Rev. Appl. **11**, 034043 (2019).

[25] R. Wang, S. He, and H. Luo, Photonic spin-Hall differential microscopy, Phys. Rev. Appl. **18**, 044016 (2022).

[26] J. Liu, Q. Yang, Y. Shou, S. Chen, W. Shu, G. Chen, S. Wen, and H. Luo, Metasurface-assisted quantum nonlocal weak-measurement microscopy, Phys. Rev. Lett. **132**, 043601 (2024).

[27] S. A. Ponomarenko, Twist phase and classical entanglement of partially coherent light, Opt. Lett. **46**, 5958 (2021).

[28] H. Jiang, P. Peng, H. Wang, X. Peng, Y. Chen, F. Wang, Y. Cai, and L. Liu, Observation of the classical entanglement of twisted partially coherent light in phase space, Opt. Lett. **50**, 7071 (2025).

[29] Y. Chen and S. A. Ponomarenko, Phase-space nonseparability, partial coherence, and optical beam shifts, Phys. Rev. Lett. **135**, 193801 (2025).

[30] R. Simon and N. Mukunda, Twisted Gaussian Schell-model beams, J. Opt. Soc. Am. A **10**, 95 (1993).

[31] A. T. Friberg, E. Tervonen, and J. Turunen, Interpretation and experimental demonstration of twisted Gaussian Schell-model beams, J. Opt. Soc. Am. A **11**, 1818 (1994).

[32] K. Sundar, R. Simon, and N. Mukunda, Twisted Gaussian Schell-model beams II spectrum analysis and propagation characteristics, J. Opt. Soc. Am. A **10**, 2017 (1993).

[33] S. A. Ponomarenko, Twisted Gaussian Schell-model solitons, Phys. Rev. E **64**, 036618 (2001).

[34] F. Gori and M. Santarsiero, Twisted Gaussian Schell-model beams as series of partially coherent modified Bessel–Gauss beams, Opt. Lett. **40**, 1587 (2015).

[35] W. J. Wild and C. L. Giles, Goos-Hänchen shifts from absorbing media, Phys. Rev. A **25**, 2099 (1982).

[36] P. T. Leung, C. W. Chen, and H.-P. Chiang, Large negative Goos–Hanchen shift at metal surfaces, Opt. Commun. **276**, 206 (2007).

[37] M. Merano, A. Aiello, G. W. 't Hooft, M. P. van Exter, E. R. Eliel, and J. P. Woerdman, Observation of Goos-Hänchen shifts in metallic reflection, Opt. Express **15**, 15928 (2007).

[38] V. J. Yallapragada, A. P. Ravishankar, G. L. Mulay, G. S. Agarwal, and V. G. Achanta, Observation of giant Goos-Hänchen and angular shifts at designed metasurfaces, Sci. Rep. **6**, 19319 (2016).

[39] N. I. Petrov, Y. M. Sokolov, V. V. Stoiakin, V. A. Danilov, V. V. Popov, and B. A. Usievich, Observation of giant angular Goos-Hanchen shifts enhanced by surface plasmon resonance in subwavelength grating, Photonics **10**, 180 (2023).

[40] S. Asiri, J. Xu, M. Al-Amri, and M. S. Zubairy, Controlling the Goos-Hänchen and Imbert-Fedorov shifts via pump and driving fields, Phys. Rev. A **93**, 013821 (2016).

[41] See Supplemental Material at http://link.aps.org/supplemental/10.1103/gwhv-fj1q for expressions for $X_{p,s}$, and $Y_{p,s}$, the derivation of Eqs. (2) and (5), as well as for $\boldsymbol{\Delta}$, $\boldsymbol{\Lambda}$, and $\boldsymbol{\Theta}$, and Table S1, which includes Refs. [42,43].

[42] J. D. Jackson, in *Classical Electrodynamics*, 4th ed. (Wiley, Hoboken, NJ, 2021).

[43] G. R. Fowles, in *Introduction to Modern Optics*, 2nd ed. (Holt, Rinehart, Winston, New York, 1975).

[44] A. Aiello, M. Merano, and J. P. Woerdman, Duality between spatial and angular shift in optical reflection, Phys. Rev. A **80**, 061801(R) (2009).

[45] R. G. van Holstein, C. U. Keller, F. Snik, and S. P. Bos, Polarization-dependent beam shifts upon metallic reflection in high-contrast imagers and telescopes, Astron. Astrophys. **677**, A150 (2023).

[46] G. Jayaswal, G. Mistura, and M. Merano, Observation of the Imbert–Fedorov effect via weak value amplification, Opt. Lett. **39**, 2266 (2014).

[47] C. M. Olaya, N. Hayazawa, M. H. Balgos, and T. Tanaka, Dynamic measurement of an angular Goos–Hänchen shift at a surface plasmon resonance in liquid, Appl. Opt. **62**, 8426 (2023).

[48] W. Kong, Y. Wan, S. Li, W. Zhao, and Z. Zheng, High-sensitivity Goos-Hanchen shift sensing based on Bloch surface wave, Sens. Actuators, A **276**, 62 (2018).

[49] H. Wang, X. Peng, H. Zhang, L. Liu, Y. Chen, F. Wang, and Y. Cai, Experimental synthesis of partially coherent beam with controllable twist phase and measuring its orbital angular momentum, Nanophotonics **11**, 689 (2022).